Quasi-free π^0 photoproduction from the bound nucleon

K. Kossert[1,a,b], M. Camen[1,a], F. Wissmann[1,b], J. Ahrens[2], J.R.M. Annand[3], H.-J. Arends[2], R. Beck[2], G. Caselotti[2], P. Grabmayr[4], O. Jahn[2], P. Jennewein[2], M.I. Levchuk[5], A.I. L'vov[6], J.C. McGeorge[3], A. Natter[4], V. Olmos de León[2], V.A. Petrun'kin[6], G. Rosner[3], M. Schumacher[1,c], B. Seitz[1,d], F. Smend[1], A. Thomas[2], W. Weihofen[1], and F. Zapadtka[1]

[1] II. Physikalisches Institut, Universität Göttingen, D-37073 Göttingen, Germany
[2] Institut für Kernphysik, Universität Mainz, D-55099 Mainz, Germany
[3] Department of Physics and Astronomy, University of Glasgow, Glasgow G12 8QQ, UK
[4] Physikalisches Institut, Universität Tübingen, D-72076 Tübingen, Germany
[5] B.I. Stepanov Institute of Physics, Belarussian Academy of Sciences, 220072 Minsk, Belarus
[6] P.N. Lebedev Physical Institute, 119991 Moscow, Russia

Abstract. Differential cross-sections for quasi-free π^0 photoproduction from the proton and neutron bound in the deuteron have been measured for $E_\gamma = 200$–400 MeV at $\theta_\gamma^{\mathrm{lab}} = 136.2°$ using the Glasgow photon tagger at MAMI, the Mainz 48 cm $\varnothing \times 64$ cm NaI(Tl) photon detector and the Göttingen SENECA recoil detector. For the proton measurements made with both liquid-deuterium and liquid-hydrogen targets allow direct comparison of "free" π^0 photoproduction cross-sections as extracted from the bound-proton data with experimental free cross-sections which are found to be in reasonable agreement below 320 MeV. At higher energies the "free" cross-sections extracted from quasi-free data are significantly smaller than the experimental free cross-sections and theoretical predictions based on multipole analysis. For the first time, "free" neutron cross-section have been extracted in the Δ-region. They are also in agreement with the predictions from multipole analysis up to 320 MeV and significantly smaller at higher photon energies.

PACS. 13.60.Le Meson production – 14.20.Dh Protons and neutrons – 25.20.Lj Photoproduction reactions

1 Introduction

Single-pion photoproduction has been a subject of extensive experimental and theoretical investigation for many decades. This reaction is one of the main sources of information on nucleon structure. It allows investigation of resonance excitations of the nucleon, especially the $\Delta(1232)$ excitation, and their photo-decay amplitudes. The pion photoproduction amplitude is used as an input when calculating pion photoproduction from heavier nuclei and in the dispersion analysis of nucleon Compton scattering. This reaction also serves as a test of our understanding of the chiral pion-nucleon dynamics. A well-known example is the demonstration that chiral perturbation theory

---

[a] Part of the Doctoral Thesis.
[b] *Present address*: Physikalisch-Technische Bundesanstalt, Bundesallee 100, D-38116 Braunschweig, Germany.
[c] e-mail: schumacher@physik2.uni-goettingen.de
[d] *Present address*: II. Physikalisches Institut der Universität Gießen, Germany.

---

accurately describes the very precise data on the S-wave multipole E_{0+} and the P-wave amplitudes of π^0 photoproduction on the nucleon in the threshold region [1,2].

Experimental investigation of pion photoproduction on the nucleon has a long history. More than seventeen thousand data points form the modern database of pion photoproduction at energies up to 2 GeV [3]. Almost all of them are data on the charged channels on both nucleons and on the $\gamma p \to \pi^0 p$ channel. The contribution of the $\gamma n \to \pi^0 n$ reaction to this base amounts to only 120 data points at energies up to 905 MeV obtained in 1970s at the Frascati synchrotron [4] and at the Tokyo synchrotron [5,6]. However, no direct measurements of quasi-free π^0 photoproduction on the neutron using a deuterium target have been carried out. Instead, the ratio $R = \mathrm{d}\sigma(\gamma d \to \pi^0 n p_s)/\mathrm{d}\sigma(\gamma d \to \pi^0 p n_s)$ was measured where p_s and n_s are the spectator proton and neutron, respectively, and used to obtain the free-neutron cross-section based on the assumption that R is a good approximation also for the ratio of the free cross-sections $\mathrm{d}\sigma(\gamma n \to \pi^0 n)/\mathrm{d}\sigma(\gamma p \to \pi^0 p)$. Though the method may

be reasonable in principle, the data points obtained from those works are of very limited precision.

Following a proposal made in ref. [7] (see also ref. [8]) an experiment has been carried out at the 855 MeV microtron MAMI-B, where the primary goal was to measure differential cross-sections for neutron Compton scattering in quasi-free kinematics using a deuterium target [9–11]. For that experiment the incident photon energy was chosen to be in the region from 200 MeV to 400 MeV. For the Compton-scattering experiment the produced π^0 mesons are a source of background photons due to their 2γ decay, which has to be eliminated in the analysis. In the present paper these events were used to obtain differential cross-sections for π^0 photoproduction from the proton and neutron bound in the deuteron. By replacing the deuterium target by a hydrogen target, π^0 photoproduction from the free proton was also measured under the same kinematic conditions. It should be noted that the present data are the first where the quasi-free events were identified through a coincidence between one of the π^0 decay photons and the recoiling nucleon.

2 Experiment

The experimental arrangement installed at the Glasgow photon tagger at MAMI [12] and outlined in fig. 1 has been described previously [9–11]. This allows us to give here only a short description. The large Mainz 48 cm $\varnothing \times 64$ cm NaI(Tl) detector [13,14] was positioned at a scattering angle of $\theta_\gamma^{\mathrm{lab}} = 136.2°$ (nominally 135°). The energy resolution of this detector is 1.5% in the Δ energy region and its detection efficiency 100%. The recoil nucleons were detected with the Göttingen SENECA detector [15] positioned at an average emission angle of $\theta_N = -18°$, thus covering the angular range corresponding to quasi-free kinematics. This angle was optimized for Compton scattering but sufficiently covers also the range required for π^0 photoproduction, where the average emission angle is $\theta_N = -15°$. Effects of the variation of the emission angle are precisely taken into account by computer simulation. A target-to-recoil detector distance of 250 cm was chosen as a compromise between the energy resolution for the time-of-flight measurement, $\Delta E_n/E_n \approx 10\%$, and the geometrical acceptance $\Delta\Omega_n \approx 90$ msr. As target a 5 cm $\varnothing \times 15$ cm Kapton cell filled with liquid deuterium was used. By filling the same cell with liquid hydrogen, it was possible to investigate quasi-free and free π^0 photoproduction on the proton under identical kinematic conditions.

SENECA consists of 30 hexagonally shaped cells filled with NE213 liquid scintillator (15 cm in diameter and 20 cm in length) mounted in a honeycomb structure. Veto-detectors in front of SENECA provided the possibility to identify charged background particles and to discriminate between neutrons and protons. This allowed clean separation between quasi-free Compton scattering and π^0 photoproduction from the proton and neutron detected in the same experiment. The detection efficiency of the veto-detectors for protons was implemented in the Monte Carlo
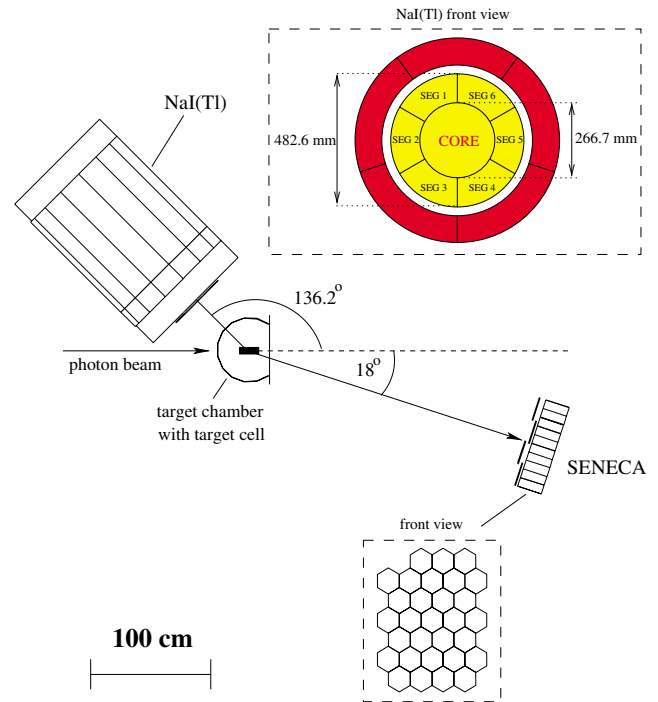

Fig. 1. The experimental setup used to measure quasi-free Compton scattering from the bound neutron and proton. The scattered photons were detected with the large-volume NaI(Tl) detector, the recoiling neutrons and protons with the SENECA detector system. Liquid deuterium and liquid hydrogen were used as target materials. The target cells are mounted in a scattering chamber having a Kapton window downstream the photon beam to reduce the energy loss of the protons on their way to SENECA.

program [16]. The detection efficiency for neutrons was measured *in situ* by analysing events from the $p(\gamma, \pi^+n)$ reaction leading to $\epsilon_n = 18\%$ [11] on the average. The new data for ϵ_n being valid on a few percent level of precision are used to correct the results of computer simulations. For further details see [11]. The momenta of the recoil nucleons were measured using the time-of-flight (TOF) technique with the NaI(Tl) detector providing the start signal and the SENECA modules providing the stop signals.

Data were collected during 238 h of beam time with a deuterium target and 35 h with a hydrogen target. The tagging efficiency, being 55%, was measured several times during the runs by means of a Pb-glass detector moved into the direct photon beam, and otherwise monitored by a P2 type ionization chamber positioned at the end of the photon beam line.

3 Data analysis

Before analysing the data obtained with the deuterium target the corresponding analysis of data obtained with the hydrogen target was carried out. In this case the separation of events from Compton scattering and π^0 photoproduction can be achieved by the NaI(Tl) detector alone,
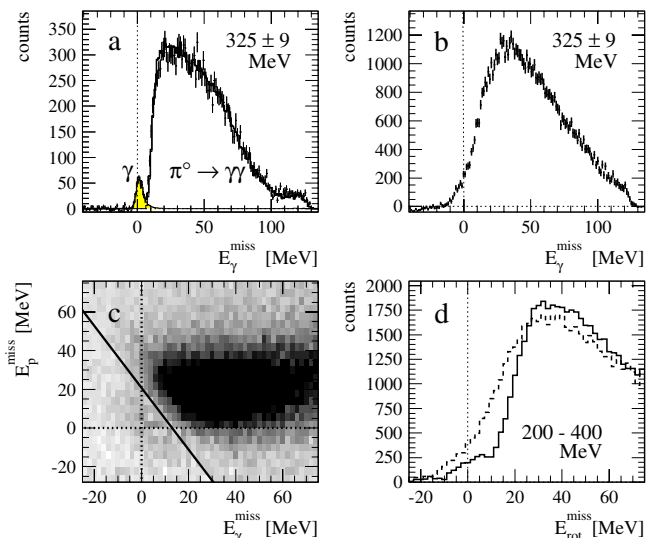
Fig. 2. Panel a: Number of proton events obtained with a hydrogen target *versus* the missing photon energy E_γ^{miss}. Panel b: The same as panel a but for proton events obtained with a deuterium target. Panel c: Scatter plot of proton events obtained with a deuterium target. Abscissa and ordinate are the missing energies of the scattered photon and the recoil proton, respectively. The thick solid line separates Compton events located in the vicinity of the origin and (γ, π^0) events shown as a dark range. For the further evaluation each point in the scatter plot was rotated (moved on a circle centered at the origin), until the thick solid line was perpendicular to the abscissa. Panel d: Projection of proton events obtained with a deuteron target after rotation (solid line) and before rotation (broken line).

but the detection of the recoiling proton improves the separation, especially for energies near the peak of the Δ-resonance. A typical spectrum is shown in panel a of fig. 2. The data obtained for the free proton have been used to optimize the analysis procedure for the bound nucleon.

For the separation of events from Compton scattering and π^0 photoproduction it is convenient to use two-dimensional scatter plots of events with the missing nucleon energy $E_N^{\text{miss}} = E_N^{\text{calc}} - E_N^{\text{SEN}}$ and the missing photon energy $E_\gamma^{\text{miss}} = E_\gamma^{\text{calc}} - E_\gamma^{\text{NaI}}$ as the parameters, where E_N^{SEN} and E_γ^{NaI} denote measured energies and E_N^{calc} and E_γ^{calc} the corresponding calculated energies. The calculations are carried out using the tagged-photon energy and the detected nucleon angle or scattered photon angle and assuming the kinematics of Compton scattering by the proton in case of a hydrogen target or the kinematics of Compton scattering in the center of the quasi-free peak [7] in case of a deuteron target. As an example, panel c of fig. 2 shows the scatter plot of proton events obtained with 200 MeV–400 MeV photons incident on a deuterium target. Two separate regions containing events are visible. The Compton events are located in a narrow zone around the origin ($E_\gamma^{\text{miss}} = 0, E_p^{\text{miss}} = 0$), the (γ, π^0) events in the dark range at larger missing energies. For the further evaluation each point in the panel was rotated (moved on a circle centered in the origin) until the thick solid line became
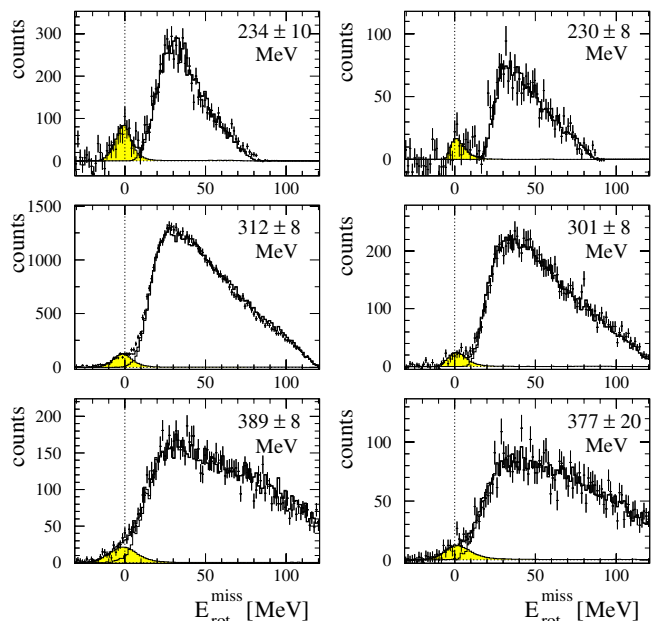

Fig. 3. Typical spectra of events obtained with the deuteron target shown for the recoil proton (left panels) and recoil neutrons (right panels). The data from the two-dimensional plot have been projected onto the abscissa after the rotation described in the caption of fig. 2 and in the text. The solid curves are the results of a Monte Carlo simulation scaled to the Compton events and the (γ, π^0) events, respectively.

perpendicular to the abscissa. This has the advantage that projections of the data on the new abscissa —denoted by $E_{\text{rot}}^{\text{miss}}$— can be used for further analysis without loss in the quality of the separation between the two types of events.

The benefits of this procedure are illustrated in fig. 2. Panel a shows numbers of proton events from a proton target *versus* the measured missing energy of the scattered photon, given for a narrow energy interval close to the maximum of the Δ-resonance. In this case, we find very good separation between the two types of events as in previous experiments carried out with proton targets. The good separation disappears when proton events of the same type are taken from a deuteron target. These data are shown in panel b, where it can clearly be seen that the effects of binding destroy the separation of the two types of events which was visible in panel a. The separation can be partly restored when the rotation procedure is applied as is shown in panel d. This panel contains as a solid line the same data as the scatter plot of events shown in panel c but projected on to the abscissa after rotation. For comparison the broken line shows the same data before rotation. The comparison of these two lines clearly demonstrates that the rotation procedure improves the separation of the two types of events.

Figure 3 shows typical spectra obtained with the deuterium target. The left panels contain proton events, the right panels neutron events. The different numbers of events on the two sides are due to the difference between the SENECA detection efficiency for neutrons ($\approx 18\%$) and protons ($\approx 99\%$). There is a reasonable separation of

the two types of events in the whole energy range. For the final separation and for the determination of the numbers of photopion events, a complete Monte Carlo simulation has been carried out for the processes under consideration. The results of these simulations shown by solid curves were scaled to the Compton and (γ, π^0) data, thus leading to the grey areas in case of the Compton-scattering events and to the white areas in case of the π^0 events.

The number of (γ, π^0) events, which is the number of events given by the adjusted curves, corresponds to the integral of the triple differential cross-section in the region of the quasi-free peak. The following relation has been used to determine the final triple differential cross-section in the center of the nucleon quasi-free peak (NQFP):

$$\left(\frac{\mathrm{d}^3\sigma}{\mathrm{d}\Omega_{\pi^0}\mathrm{d}\Omega_N\mathrm{d}E_N}\right)_{\mathrm{NQFP}} = \frac{N_{\pi^0 N}}{N_\gamma N_T \, \epsilon_N R_{\mathrm{NQFP}}^{\gamma\pi^0}}, \quad (1)$$

where $N_{\pi^0 N}$ is the number of coincident π^0-nucleon events as extracted from the missing energy spectra, N_γ is the number of incident photons, N_T is the number of target nuclei, ϵ_N is the nucleon detection efficiency and $R_{\mathrm{NQFP}}^{\gamma\pi^0}$ is a factor obtained by Monte Carlo simulation which relates the number of (γ, π^0) events integrated over the distribution of events to the triple differential cross-section in the center of the nucleon quasi-free peak.

4 Theory

In our analysis of the data we used the theoretical model proposed in refs. [17,18] and developed subsequently in refs. [19–21] (see also refs. [22,23]). The model is based on the diagrams relevant for the reaction on the kinematic conditions under consideration. The main graphs contributing to the reaction amplitude in the quasi-free region are displayed in fig. 4. Graph 4a) describes quasi-free photoproduction from the nucleon N_1. It is expected to be dominant when the momentum of the nucleon N_2 is sufficiently small ($\lesssim \sqrt{mE_b}$, where $E_b = 2.2246$ MeV is the deuteron binding energy and m the nucleon mass). This corresponds to the so-called nucleon quasi-free peak (NQFP) region. The non-interacting nucleon N_2 in this graph is often referred to as the spectator.

The final nucleons can interact with each other through the mechanism displayed in graph 4b), describing the so-called final-state interaction (FSI). This graph was found to be of great importance for many processes involving deuteron disintegration, including the reaction $\gamma d \to \pi NN$ (see refs. [17–21,23]). The big effect of FSI is mainly caused by NN interaction in the s-wave at small relative momenta ($\lesssim 200$ MeV/c) of the NN pair. Such small relative momentum is provided under the kinematic conditions of small incident energies and/or forward angles of a third particle in the final state, which is the pion in our case. Of the two s-wave final states, $^1S_0$ and $^3S_1$, the repulsive isosinglet np-wave $^3S_1$ proved to be the more important one, leading to a decrease of the cross-section due to FSI. Experiments on semi-inclusive π^0 photoproduction in the reaction $d(\gamma, \pi^0)np$ [24,25] clearly confirm
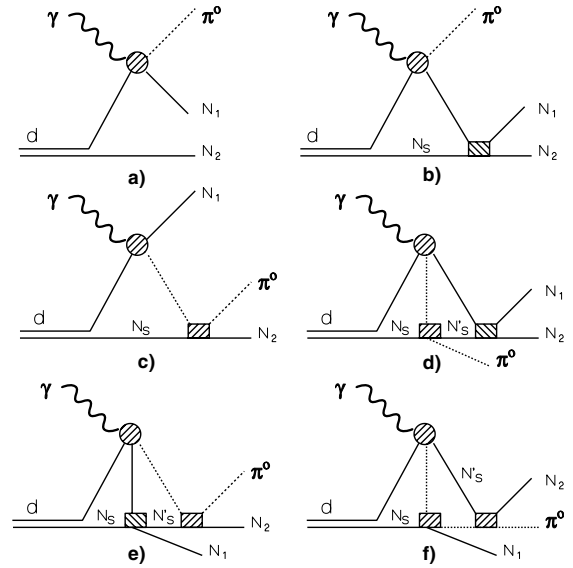

Fig. 4. Graphs contributing to the reaction $\gamma d \to \pi^0 np$. The set of graphs where $N_1 \leftrightarrow N_2$ is not shown in the figure.

these properties of FSI. Since our experiment covers the kinematic region where the relative momentum of the np pair ranges from 140 to 270 MeV/c, we expect that FSI gives a noticeable contribution at the beginning of the energy interval and decreases in importance with increasing photon energy.

The pion (neutral or charged) produced in the $\gamma N \to \pi N$-vertex can be scattered by the spectator nucleon as displayed in graph 4c). Although the detailed investigation of the reaction $\gamma d \to \pi^- pp$ performed in refs. [17, 18] has shown that there exists a kinematic region where the diagram 4c) can give a noticeable contribution to the amplitude in the Δ-region, usually the effect of πN rescattering is smaller than that of NN rescattering. In our previous paper [19] we found the contribution of graph 4c) in the NQFP region to be of minor importance at energies from 250 to 400 MeV.

It is known that two-loop diagrams can be important for the description of the reaction $\gamma d \to \pi NN$ under certain kinematic conditions. For instance, the graph 4d) proved to give a big contribution to the inclusive process $d(\gamma, \pi^0)np$ in the threshold region (see ref. [20]). This result can be easily understood if one takes into account that the threshold electric-dipole amplitude E_{0+} of charged-pion photoproduction, which is contained in the upper block of this graph, is about 30 times larger in absolute numbers than those for neutral channels. With increasing photon energy, this effect is expected to decrease in importance. Nevertheless, we will take it into account.

A significant modification of the reaction amplitude through s-wave interaction of the NN pair may not only occur in the final state but also in the intermediate state by the mechanism displayed in graph 4e). This was previously demonstrated in refs. [17,18] in the analysis of the reaction $\gamma d \to \pi^- pp$, where it was shown that of the two possible s-wave interactions, $^1S_0$ and $^3S_1$, the isosinglet $^3S_1$-state is dominant. We have observed the same

result in our model. It should be noted that, for example in the pQFP region, almost the total contribution from the graph 4e) stems from the configuration where the nucleon N_1 is the neutron, *i.e.* this nucleon has a small momentum. In such a situation, the kinematics allows both the deuteron wave function (DWF) and np scattering amplitude to act simultaneously in the low momentum regime where they are strongly enhanced.

There is one further two-loop contribution due to πN rescattering both in the intermediate and final states and this is displayed in diagram 4f). Since the πN scattering amplitude is smaller than the NN scattering amplitude we expect this diagram to be less important in comparison with, *e.g.*, diagram 4d). Below we will see that the latter gives only a few percent contribution to the differential cross-section. Therefore, the diagram 4f) can safely be disregarded. The smallness of the contribution of this diagram to the amplitude of the reaction $\gamma d \to \pi^- pp$ in the Δ-region was also mentioned in refs. [17,18].

All details of the calculations in the extended model, *i.e.* including the graphs c) to f) of fig. 4, will be published elsewhere [26]. Here we mention only the following. The pion photoproduction amplitude was taken in the on-shell form and calculated with the SAID [27] and MAID [28] multipole analyses. Below we will use the most recent SAID SM02K and MAID DMT2001 solutions. The off-shell corrections are expected to be small in the NQFP region so that the use of the on-shell parametrization for the amplitudes is quite justified.

A model of the NN interaction is needed to calculate the DWF and the NN scattering amplitude when evaluating the diagrams. We checked three versions of the Bonn OBEPR model [29,30], the CD-Bonn potential [31], and a separable approximation [32,33] of the Paris potential [34]. Our observation is that the results obtained with all the potentials are practically the same so that in the following we will present our results with the most recent of them, namely with the CD-Bonn model.

The πN scattering amplitude was calculated in a meson-exchange model [35,36] constructed in the three-dimensional Bethe-Salpeter formulation. To take into account the off-shell nature of the intermediate pion, we supply its propagator by a dipole-like form factor, $F_\pi(q_{on}, q_{off}) = (\Lambda_\pi^2 + q_{on}^2)^2/(\Lambda_\pi^2 + q_{off}^2)^2$ with q_{on} (q_{off}) being the on-shell (off-shell) momentum of the intermediate pion. Introducing the form factor ensures also the convergence of the integrals over the pion off-shell momentum $\mathbf{q}_{off}$ which emerges in the evaluations of graphs 4c)-d). The value of the cut-off parameter Λ_π is usually treated as a free parameter which is adjusted to provide the best description of the reaction under consideration. It is not surprising that in the literature there exists a great variety of numerical values for Λ_π. We use two different choices for it. The first one is a very soft form-factor ($\Lambda_\pi = 440$ MeV) which was used in refs. [37,38] to give the best fits to the π^0 photo and electroproduction data in the threshold region as well as to the $\Delta(1232)$ resonance multipole $M_{1+}^{(3/2)}$ over a wide energy range. The second one is a very hard form-factor ($\Lambda_\pi = 1720$ MeV) used
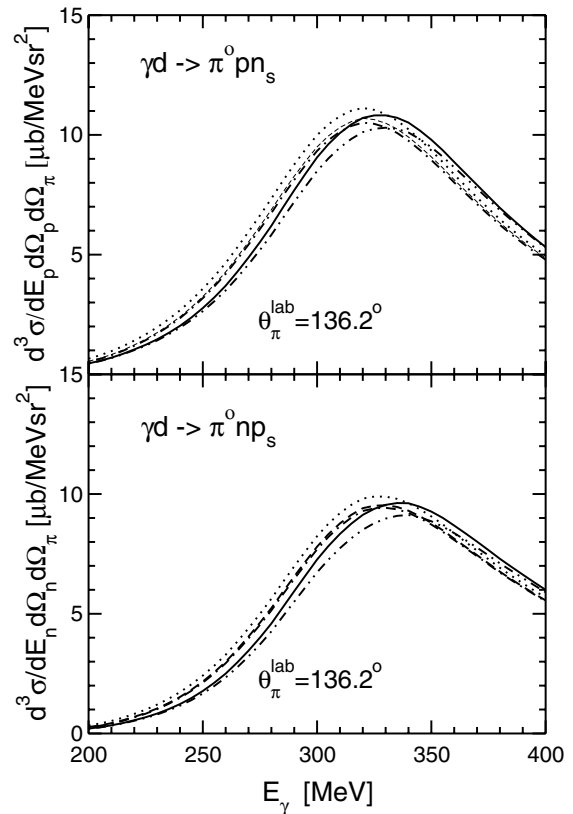

Fig. 5. Contributions of the graphs in fig. 4 to the triple differential cross-section of the reaction $\gamma d \to \pi^0 np$ in the CpQFP (upper figure) and the CnQFP (lower figure). Dotted curves: pole proton (upper figure) and neutron (lower figure) diagrams (graph 4a). Successive addition of graphs 4b), d), and e) gives the dashed, dash-dotted, and solid lines, respectively. The contribution from graph 4c) is small and is not shown in the figure. All the curves are obtained for $\Lambda_\pi = 440$ MeV. The total results for $\Lambda_\pi = 1720$ MeV is shown in dash-double-dotted curves.

in ref. [31] for the construction of the CD-Bonn potential. We found, however, that the variation of Λ_π from 1000 MeV to 1720 MeV practically does not change the results. Moreover, for $\Lambda_\pi > 1000$ MeV, one can safely put the form factor $F_\pi(q_{on}, q_{off})$ to be equal to 1. In actual calculations, the upper limit of the integrals was taken to be $p^{max} = 1000$ MeV/c but its replacement by $p^{max} = 500$ MeV/c changed the cross-sections by less than 3%.

Contributions of separate diagrams to the triple differential cross-section of the reaction $\gamma d \to \pi^0 np$ are shown in fig. 5. The effect of FSI manifests itself in a noticeable reduction of the cross-section. The size of this reduction ranges from 20% at 200 MeV, and 5% at 300 MeV, to 2% at 400 MeV in the center of the proton quasi-free peak (CpQFP). In the center of the neutron quasi-free peak (CnQFP), one has the same numbers. It is interesting to note that the numbers given above were also obtained by us for the relative FSI contribution in the case of the reaction $\gamma d \to \gamma' np$ [11]. The effect of πN rescattering (graph 4c)) does not exceed 1% and is not shown in fig. 5. The inclusion of graph 4d) leads to a
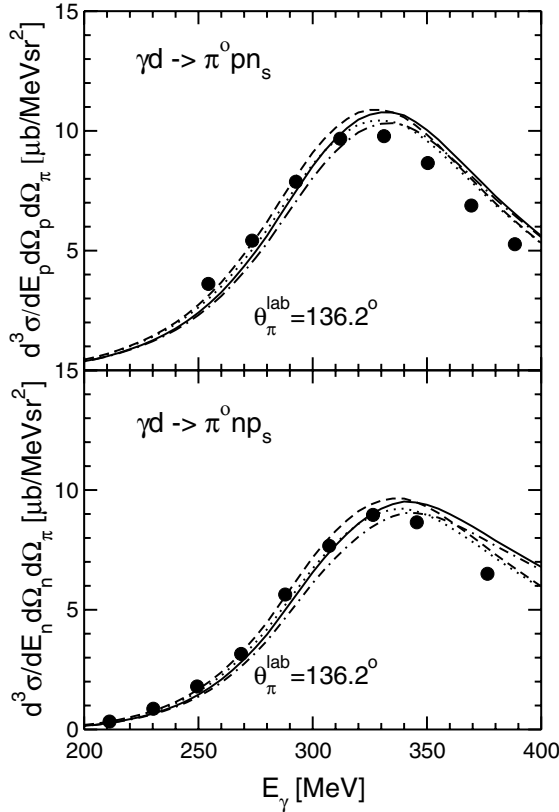
Fig. 6. Triple differential cross-section of the reaction $d(\gamma, \pi^0 p)n$ (upper figure) and $d(\gamma, \pi^0 n)p$ (lower figure) in the center of the NQFP at $\theta_\pi^{\mathrm{lab}} = 136.2°$. Results for the MAID2001 solution are shown in dash-dotted (with $\Lambda_\pi = 440$ MeV) and solid (at $\Lambda_\pi = 1720$ MeV) curves. Corresponding results for the SM02K solution are given in dashed and dotted curves.

Table 1. The energy dependence of the triple differential cross-section of the reaction $d(\gamma, \pi^0 p)n$ in CpQFP at $\theta_\pi^{\mathrm{lab}} = 136.2°$. The statistical error is given. The systematic experimental error amounts to 4.4%.

E_γ (MeV)	$\left(\frac{\mathrm{d}^3\sigma}{\mathrm{d}\Omega_\pi \mathrm{d}\Omega_p \mathrm{d}E_p}\right)^{\mathrm{CpQFP}}$ $\left(\frac{\mu\mathrm{b}}{\mathrm{MeV\ sr^2}}\right)$
254.3	3.61 ± 0.04
273.5	5.42 ± 0.05
292.7	7.88 ± 0.05
312.0	9.67 ± 0.06
331.2	9.78 ± 0.07
350.4	8.66 ± 0.09
369.4	6.88 ± 0.09
388.5	5.27 ± 0.08

decrease of the cross-section by 6% at 200 MeV, 2% at 300 MeV, and 0.5% at 400 MeV. These numbers are practically independent of the Λ_π value. A further reduction of the cross-section below 320 MeV is due to the contribution of diagram 4e). The reduction is quite visible, being about 15% from 200 to 260 MeV and reducing further to 8% at 300 MeV. These numbers are obtained for $\Lambda_\pi = 1720$ MeV. For $\Lambda_\pi = 440$ MeV they are 12% and 2%,

Table 2. The energy dependence of the triple differential cross-section of the reaction $d(\gamma, \pi^0 n)p$ in CnQFP at $\theta_\pi^{\mathrm{lab}} = 136.2°$. The statistical error is given. The systematic experimental error amounts to 9.0%.

E_γ (MeV)	$\left(\frac{\mathrm{d}^3\sigma}{\mathrm{d}\Omega_\pi \mathrm{d}\Omega_n \mathrm{d}E_n}\right)^{\mathrm{CnQFP}}$ $\left(\frac{\mu\mathrm{b}}{\mathrm{MeV\ sr^2}}\right)$
211.1	0.33 ± 0.02
230.2	0.87 ± 0.03
249.4	1.80 ± 0.04
268.7	3.15 ± 0.06
287.9	5.64 ± 0.08
307.2	7.67 ± 0.10
326.4	8.96 ± 0.12
345.6	8.65 ± 0.15
376.5	6.50 ± 0.11

respectively. Above 320 MeV, one observes some increase of the cross-section after inclusion of graph 4e). The total contribution of one-loop and two-loop diagrams is -30%, -15%, and $+6\%$ at 200, 300, and 400 MeV, respectively, if one takes 1720 MeV for Λ_π. With $\Lambda_\pi = 440$ one has almost the same numbers at 200 and 400 MeV but at 300 MeV the decrease of the cross-section is noticeably smaller being about -9%.

The measured triple differential cross-section, $\mathrm{d}^3\sigma/\mathrm{d}\Omega_\pi \mathrm{d}\Omega_p \mathrm{d}E_p$ (here E_p and Ω_p are the kinetic energy and solid angle of the proton, respectively), in the CpQFP can be related to the differential cross-section of pion photoproduction on the "free" nucleon, $\mathrm{d}\sigma/\mathrm{d}\Omega_\pi$, via the spectator formula

$$\frac{\mathrm{d}\sigma(\gamma p \to \pi^0 p)}{\mathrm{d}\Omega_\pi} =$$

$$\frac{(2\pi)^3}{u^2(0)} \frac{E_\gamma |\mathbf{q}_\pi|^2}{|\mathbf{p}_p| E_\gamma^{\mathrm{f}}(\varepsilon_\pi q_\pi \cdot p_p - \varepsilon_p \mu^2)} \frac{\mathrm{d}^3\sigma(\gamma d \to \pi^0 pn)}{\mathrm{d}\Omega_\pi \mathrm{d}\Omega_p \mathrm{d}E_p}, \quad (2)$$

where $u(0)$ is the S-wave amplitude of the DWF at zero momentum (the D-wave component of this function does not contribute at zero momentum), q_π is the pion 4-momentum, μ is the pion mass, p_p is the proton 4-momentum. E_γ^{f} is the lab photon energy corresponding to the free-pion photoproduction

$$E_\gamma^{\mathrm{f}} = \frac{(p_p + q_\pi)^2 - m^2}{2m} = E_\gamma - E_{\mathrm{b}}\left(1 + \frac{E_\gamma - E_{\mathrm{b}}/2}{m}\right). \quad (3)$$

In the case of quasi-free pion photoproduction on the neutron, one has a formula analogous to that of eqs. (2) and (3) but with the replacement $p \leftrightarrow n$.

Equation (2) is valid for the pole diagram contribution (fig. 4a) only. Therefore, in order to make eq. (2) valid for practical applications the r.h.s. of this equation has to be multiplied by a factor $f(E_\gamma, \theta_\gamma) = \mathrm{d}^3\sigma_{\mathrm{pol}}/\mathrm{d}^3\sigma_{\mathrm{tot}}$ (see analogous discussion in ref. [11]). Here, $\mathrm{d}^3\sigma_{\mathrm{pol}}$ stands for the contribution of the pole (proton or neutron) diagram to the total differential cross-section $\mathrm{d}^3\sigma_{\mathrm{tot}}$ for which all the diagrams a)-f) have been taken into account.

Table 3. The energy dependence of the differential cross-section of "free" proton π^0 photoproduction extracted from quasi-free data at $\theta_\pi^{\mathrm{lab}} = 136.2°$. The statistical error is given. The systematic experimental error amounts to 4.4%. The error of the conversion of quasi-free cross-sections to "free" cross-sections amounts to 4%.

E_γ^{f} (MeV)	$\frac{\mathrm{d}\sigma}{\mathrm{d}\Omega_\pi^{\mathrm{lab}}}$ $\left(\frac{\mu\mathrm{b}}{\mathrm{sr}}\right)$	θ_π^{cm} (degrees)	$\frac{\mathrm{d}\sigma}{\mathrm{d}\Omega_\pi^{\mathrm{cm}}}$ $\left(\frac{\mu\mathrm{b}}{\mathrm{sr}}\right)$
251.5	5.43 ± 0.06	146.7	8.54 ± 0.09
270.6	7.07 ± 0.06	146.8	11.23 ± 0.10
289.8	8.73 ± 0.05	147.1	14.04 ± 0.08
309.0	9.84 ± 0.06	147.3	16.04 ± 0.10
328.2	8.12 ± 0.06	147.6	13.42 ± 0.10
347.3	6.36 ± 0.07	147.8	10.67 ± 0.12
366.3	4.59 ± 0.06	148.1	7.82 ± 0.10
385.4	3.26 ± 0.05	148.4	5.64 ± 0.09

Table 4. The energy dependence of the differential cross-section of "free" neutron π^0 photoproduction extracted from the quasi-free data at $\theta_\pi^{\mathrm{lab}} = 136.2°$. The statistical error is given. The systematic experimental error amounts to 9.0%. The error of the conversion of quasi-free to "free" cross sections amounts to 4%.

E_γ^{f} (MeV)	$\frac{\mathrm{d}\sigma}{\mathrm{d}\Omega_\pi^{\mathrm{lab}}}$ $\left(\frac{\mu\mathrm{b}}{\mathrm{sr}}\right)$	θ_π^{cm} (degrees)	$\frac{\mathrm{d}\sigma}{\mathrm{d}\Omega_\pi^{\mathrm{cm}}}$ $\left(\frac{\mu\mathrm{b}}{\mathrm{sr}}\right)$
208.4	0.78 ± 0.04	146.7	1.22 ± 0.08
227.4	1.68 ± 0.05	146.5	2.62 ± 0.09
246.6	3.02 ± 0.06	146.6	4.74 ± 0.11
265.8	4.53 ± 0.08	146.8	7.17 ± 0.14
285.0	6.86 ± 0.09	147.0	10.99 ± 0.16
304.3	8.11 ± 0.10	147.2	13.17 ± 0.18
323.4	8.07 ± 0.10	147.5	13.29 ± 0.18
342.6	6.80 ± 0.12	147.7	11.36 ± 0.20
373.4	4.34 ± 0.08	148.2	7.43 ± 0.12

5 Discussion of the results

Results for the triple differential cross-section of the reactions $d(\gamma, \pi^0 p)n$ and $d(\gamma, \pi^0 n)p$ in CpNQFP and CnQFP at $\theta_\pi^{\mathrm{lab}} = 136.2°$ are given in tables 1 and 2, respectively, and displayed in fig. 6. Also in this figure we show theoretical predictions in the framework of the model described above. The area filled by the curves gives the size of uncertainties of the theoretical model. One can see good agreement between the experimental data and theoretical predictions below 320 MeV. This agreement, however, vanishes above the Δ-peak. At present, we do not know the reasons responsible for the disagreement. For instance, the effect of $N\Delta$ interaction omitted in our theoretical model was shown in ref. [39] to be of no importance in the Δ-region at backward angles. Further theoretical efforts are needed to shed light on the above situation.

Using eq. (2) with the correction factor $f(E_\gamma, \theta_\gamma)$ included, we can extract the free-nucleon cross-sections from the corresponding quasi-free data. It should be noted that the extracted free values are practically independent of the choice of the multipole analysis of pion photoproduction, so that the only model dependence in these values stems from their sensitivity to the cut-off parameter Λ_π.
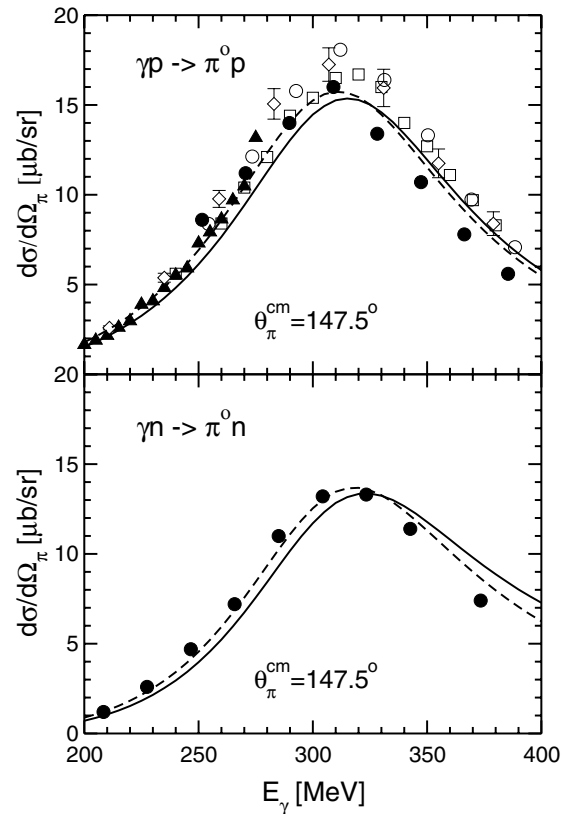

Fig. 7. The CM differential cross-section of the free proton (upper figure) and free neutron (lower figure) at $\theta_\pi^{\mathrm{cm}} = 147.5°$. The present free data measured with the hydrogen target are shown as open circles. Present "free" data extracted from cross-sections for the bound nucleon are shown as filled circles. Also shown are the available data from hydrogen targets from refs. [40] ($\square$), [41] ($\blacktriangle$), and [42] ($\diamond$) measure with a hydrogen target. The solid and dashed curves represent results obtained from the MAID2001 and SM02K solutions, respectively.

After averaging over two sets of results for $\Lambda_\pi = 440$ and 1720 MeV we obtain the central numbers given in tables 3 and 4 and displayed in fig. 7 to which an uncertainty of about 4% due to the conversion from quasi-free to "free" according to eq. (2) should be attributed. In fig. 7 we also show the cross-sections measured with the hydrogen target (see table 5) and compare them with the data obtained in other experiments [40–42] and with the predictions of the multipole analyses. Reasonable agreement between all data sets is seen up to the Δ-peak. All of them fairly well correspond to the SM02K solution and are slightly above the predictions of the MAID2001 solution. However, above 320 MeV our quasi-free data points for the proton lie significantly below both all the free data and the multipole predictions. Of course, this has to be expected from the unsatisfactory description of the quasi-free data above 320 MeV mentioned above. The free-neutron cross-sections are consistent with the multipole predictions at all energies except for 377 MeV where the measured value is noticeably smaller than the predicted one.

Table 5. The energy dependence of the differential cross-section of the reaction $p(\gamma, \pi^0)p$ at $\theta_\pi^{\mathrm{lab}} = 136.2°$. The statistical error is given. The systematic experimental error amounts to 4.4%.

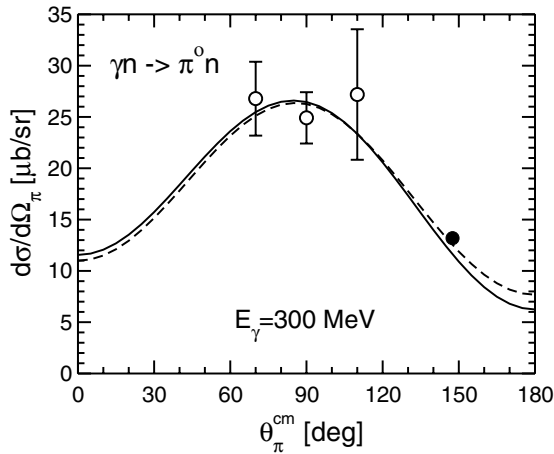| E_γ (MeV)	$\frac{d\sigma}{d\Omega_\pi^{\mathrm{lab}}}$ $\left(\frac{\mu b}{sr}\right)$	θ_π^{cm} (degrees)	$\frac{d\sigma}{d\Omega_\pi^{cm}}$ $\left(\frac{\mu b}{sr}\right)$
254.3	5.32 ± 0.08	146.7	8.38 ± 0.13
273.5	7.62 ± 0.11	146.9	12.13 ± 0.18
292.7	9.79 ± 0.10	147.1	15.77 ± 0.16
312.0	11.06 ± 0.12	147.3	18.07 ± 0.20
331.3	9.89 ± 0.10	147.6	16.39 ± 0.17
350.4	7.91 ± 0.09	147.9	13.31 ± 0.15
369.4	5.70 ± 0.08	148.1	9.74 ± 0.14
388.5	4.08 ± 0.07	148.4	7.08 ± 0.12
407.4	2.96 ± 0.06	148.7	5.22 ± 0.11
427.3	2.10 ± 0.05	149.0	3.76 ± 0.09
448.3	1.46 ± 0.04	149.3	2.66 ± 0.07
469.0	1.11 ± 0.04	149.5	2.06 ± 0.07

Fig. 8. The angular dependence of the CM differential cross-section of the reaction $\gamma n \to \pi^0 n$ at 300 MeV. The present data point is shown as a filled circle. Data from ref. [6] are shown as empty circles. Solid and dashed curves represent results of the MAID2001 and SM02K solutions, respectively.

As has been mentioned in the introduction, the experimental information on the $\gamma n \to \pi^0 n$ channel is very sparse. Up to now, there has been only one measurement of the differential cross-section in the Δ-region [6] which covered the angular region from 70° to 130°. In fig. 8 we show the angular distribution of the cross-section at 300 MeV. One can see that the data from [6] and from the present paper are consistent with each other in the sense that they are in agreement with the predictions of the same multipole analyses. But a significant improvement in the accuracy of the present experiment in comparison with that of ref. [6] is evident.

6 Conclusion

The energy dependence of the triple differential cross-section for π^0 photoproduction from the proton and neutron in deuterium and the free photoproduction cross-section from the proton have been measured in the same kinematics at $\theta^{\mathrm{lab}} = 136.2°$. For the first time accurate "free" cross-sections have been extracted for the proton and the neutron from the quasi-free data in the Δ-region, using an extended model for the conversion developed in the present work. Applying this model to the proton, "free" cross-sections are found to be in good agreement with the present and previously measured free cross-sections and in reasonable agreement with theoretical predictions based on multipole analyses below 320 MeV. For the neutron no previous data are available to compare with. The "free" neutron cross-sections obtained here also reasonably agree with theory up to 320 MeV. At higher energies there is significant disagreement for both proton and neutron which is not presently understood.

References

1. A. Schmidt *et al.*, Phys. Rev. Lett. **87**, 232501 (2001).
2. V. Bernard, N. Kaiser, U.-G. Meißner, Z. Phys. C **70**, 483 (1996).
3. See the SAID database at the website http://gwdac.phys.gwu.edu.
4. C. Bacci *et al.*, Phys. Lett. B **39**, 559 (1972).
5. Y. Hemmii *et al.*, Nucl. Phys. B **55**, 333 (1973).
6. A. Ando *et al.*, Physik Daten, 1977, unpublished.
7. M.I. Levchuk, A.I. L'vov, V.A. Petrun'kin, preprint FIAN No. 86 (1986); Few-Body Syst. **16**, 101 (1994).
8. F. Wissmann, M.I. Levchuk, M. Schumacher, Eur. Phys. J. A **1**, 193 (1998).
9. K. Kossert *et al.*, Phys. Rev. Lett. **88**, 162301 (2002).
10. M. Camen *et al.*, Phys. Rev. C **65**, 032202 (2002).
11. K. Kossert *et al.*, Eur. Phys. J. A **16**, 259 (2003).
12. I. Anthony, J.D. Kellie, S.J. Hall, G.J. Miller, Nucl. Instrum. Methods A **301**, 230 (1991); S.J. Hall, G.J. Miller, R. Beck, P. Jennewein, Nucl. Instrum. Methods A **368**, 698 (1996).
13. F. Wissmann *et al.*, Phys. Lett. B **335**, 119 (1994).
14. F. Wissmann *et al.*, Nucl. Phys. A **660**, 232 (1999).
15. G. v. Edel *et al.*, Nucl. Instrum. Methods A **332**, 224 (1993).
16. R. Brun *et al.*, GEANT Detector Description and Simulation Tool, CERN Program Library Long Writeup W5013, Cern Geneva Switzerland (1994), http://wwwinfo.cern.ch/asd/geant/index.html.
17. J.M. Laget, Nucl. Phys. A **296**, 388 (1978).
18. J.M. Laget, Phys. Rep. **69**, 1 (1981).
19. M.I. Levchuk, V.A. Petrun'kin, M. Schumacher, Z. Phys. A **355**, 317 (1996).

20. M.I. Levchuk, M. Schumacher, F. Wissmann, Nucl. Phys. A **675**, 621 (2000).
21. M.I. Levchuk, M. Schumacher, F. Wissmann, nucl-th/0011041.
22. R. Schmidt, H. Arenhövel, P. Wilhelm, Z. Phys. A **355**, 421 (1996).
23. E.M. Darwish, H. Arenhövel, M. Schwamb, Eur. Phys. J A **16**, 111 (2003).
24. B. Krusche *et al.*, Eur. Phys. J. A **6**, 309 (1999).
25. U. Siodlaczek *et al.*, Eur. Phys. J. A **10**, 365 (2001) and U. Siodlaczek, PhD Thesis, University of Tübingen, 2000.
26. M.I. Levchuk, M. Schumacher, F. Wissmann, in preparation.
27. R.A. Arndt, W.J. Briscoe, I.I. Strakovsky, R.L. Workman, Phys. Rev. C **66**, 055213 (2002) and the code SAID.
28. D. Drechsel, O. Hanstein, S.S. Kamalov, L. Tiator, Nucl. Phys. A **645**, 145 (1999) and the code MAID.
29. R. Machleidt, K. Holinde, Ch. Elster, Phys. Rep. **149**, 1 (1987).
30. R. Machleidt, Adv. Nucl. Phys. **19**, 189 (1989).
31. R. Machleidt, Phys. Rev. C **63**, 024001 (2001).
32. J. Haidenbauer, W. Plessas, Phys. Rev. C **30**, 1822 (1984).
33. J. Haidenbauer, W. Plessas, Phys. Rev. C **32**, 1424 (1985).
34. M. Lacombe *et al.*, Phys. Rev. D **12**, 1495 (1975).
35. C.T. Hung, S.N. Yang, T.-S.H. Lee, J. Phys. G **20**, 1531 (1994).
36. C.T. Hung, S.N. Yang, T.-S.H. Lee, Phys. Rev. C **64**, 034309 (2001).
37. S.S. Kamalov, S.N. Yang, Phys. Rev. Lett. **83**, 4494 (1999).
38. S.S. Kamalov *et al.*, Phys. Lett. B **522**, 27 (2001).
39. I.T. Obukhovsky *et al.*, nucl-th/0212110.
40. H. Genzel *et al.*, Z. Phys. **268**, 43 (1974).
41. M. Fuchs *et al.*, Phys. Lett. B **368**, 20 (1996).
42. F. Härter, PhD Thesis, Mainz University, 1996.